Comparison of the April 29, 1998 M6.8 and November 5, 1998 M8.4 Flares

Haimin Wang, Philip R. Goode, Carsten Denker, Guo Yang and Vasyl Yurchishin

Big Bear Solar Observatory, New Jersey Institute of Technology
40386 North Shore Lane, Big Bear City, CA 92314-9672; haimin@solar.njit.edu

Nariaki Nitta

Lockheed Martin Solar and Astrophysics Laboratory

Joseph B. Gurman

Goddard Space Flight Center, NASA

Chris St. Cyr

Computational Physics, Inc., Naval Research Laboratory

Alexander G. Kosovichev

W.W. Hansen Experimental Physics Laboratory, Stanford University

Version on January 17, 2000

Received ________________________; accepted ________________________

ABSTRACT

We combined, and analyzed in detail, the Hα and magnetograph data from Big Bear Solar Observatory (BBSO), full-disk magnetograms from Michelson Doppler Imager (MDI) on board Solar and Heliospheric Observatory (SOHO), coronagraph data from Large Angle Spectrometric Coronagraph (LASCO) of SOHO, FeXII 195Å data from Extreme ultraviolet Imaging Telescope (EIT) of SOHO and Yohkoh Soft X-ray Telescope (SXT) data of the M6.8 flare of April 29, 1998 in National Oceanic and Atmospheric Administration (NOAA) Region 8375 and the M8.4 flare of November 5, 1998 in NOAA Region 8384.

These two flares have remarkable similarities:

(1) Partial halo Coronal Mass Ejections (CMEs) were observed for both events. For the April 29, 1998 event, even though the flare occurred in the S-E of the disk center, the ejected material predominantly moved across the equator, and the central part of the CME occurred in the N-E limb. The direction in which the cusp points in the post-flare SXT images determines the dominant direction of the CMEs. (2) Coronal dimming was clearly observed in EIT FeXII 195Å for both, but not observed in Yohkoh SXT for either event. Dimming started two hours before the onset of the flares, indicating large scale coronal restructuring before both flares. (3) No global or local photospheric magnetic field change was detected from either event; in particular, no magnetic field change was found in the dimming areas. (4) Both events lasted several hours, and, thus, could be classified as long duration events (LDEs).

However, they are different in the following important aspects:

For the April 29, 1998 event, the flare and the CME are associated with an erupting filament in which the two initial ribbons were well-connected, and then gradually separated. SXT pre-flare images show the classical S-shape sheared configuration (sigmoid structure). For the November 5, 1998 event, two initial ribbons were well separated, and the SXT pre-flare image shows the interaction of at least two loops. In

addition, no filament eruption was observed.

We conclude that even though those two events resulted in the similar coronal consequences, they are due to two distinct physical processes: eruption of sheared loops and interaction of two loops.

1. INTRODUCTION

A solar Coronal Mass Ejection (CME) represents a large scale re-arrangement of the Sun's magnetic structure which can lead to a coronal transient in the interplanetary medium. Each CME may carry away a mass of up to 10^{13} kg and release up to 10^{25} J of energy from the coronal magnetic fields (Harrison, 1991, 1994 and 1995). CMEs have been studied using a number of coronagraphs since the 1970s, e.g. Skylab, Solwind and SMM. Filament eruptions and solar flares may be local events which are associated with CMEs, however, the connection remains to be established. As a matter of fact, most observations failed to establish a systematic correlation among the onset of solar flares, prominence eruptions and CMEs (Verma, 1990; Feynman and Hundhausen, 1994; Harrison, 1995; McAllister et al., 1996; Yang and Wang, 1999). One of the difficulties in establishing a possible relationship between filament eruptions and CMEs is that CMEs are more likely to be detected if they are limb events; while filament eruptions are more easily visible as disk events. Any search for a correlation between filament eruptions and CMEs needs to be able to consider both disk and limb CMEs, and their attendant phenomena. The launch of a new generation coronagraph – the Large Angle Spectroscopic Coronagraph (LASCO) on board Solar and Heliospheric Observatory (SOHO, Domingo, Fleck and Poland, 1995), provides the most advanced tool to study the dynamics of coronal structure (Brueckner et al., 1995). LASCO comprises three coronagraphs (C1, C2 and C3), extending from 1.1 to 30 solar radii. The white light instruments (C2 and C3) not only provide excellent observations of limb CME events, but also have the sensitivity to detect the "halo" from the disk events after the CME material moves beyond the edge of the occulting disk. Halo events (including "partial" halo events) are related to the Earth-directed CMEs, and the first of this kind of events was reported by Howard et al. (1982), using observations made with the Solwind coronagraph on the P78-1 spacecraft. Several halo events have been reported by LASCO (Plunkett et al., 1998, Thompson et al., 1998; Zarro et al., 1999), two additional events are studied in this paper.

Disk coronal dimmings have been detected recently in association with halo events detected with the Yohkoh Soft X-ray Telescope (SXT, Tsuneta et al., 1991) and SOHO Extreme Ultraviolet

Telescope (EIT, Delaboudiniere et al., 1995), see e.g. Gopalswamy and Hanaoka (1998), Sterling and Hudson (1997) and Thompson et al. (1998). One interpretation is that those transient dimmings track the loss of the coronal mass which is swept into the CMEs.

At the end of 1995, Big Bear Solar Observatory (BBSO) started its new generation of full disk Hα observations. Every minute, a full disk Hα image is recorded by a 2048×2048 Kodak 8-bit Megaplus camera with the 8-inch Singer-Link telescope. The pixel size of the images is roughly $1''$, which yields a spatial resolution of $2''$. Because of BBSO's long-lasting clear skies and good seeing conditions, these movies provide an unique tool to monitor filaments continuously during their disk passage. Daily LASCO and EIT mpeg movies are now on line, facilitating the comparison with BBSO movies. In addition, high resolution Hα and magnetograph movies provide important information on the morphology of active regions and flares.

In this paper, we present comprehensive data sets of two M class flares and associated CMEs, by combining data from BBSO, SOHO and Yohkoh. We will first briefly describe the observations, then the differences and similarities between the two events, and finally present discussions of the physics of these two events deduced from our observations.

2. OBSERVATIONS AND DATA REDUCTION

The two flares under discussion are the only upper M-class events in our data archive which had complete coverage in BBSO (Hα and magnetograms), LASCO, MDI, EIT and SXT. Table 1 lists the basic properties of the flares:

EDITOR: PLACE TABLE 1 HERE.

2.1. SOHO Observations

The data we analyzed are from three of the payload instruments of SOHO:

(1) LASCO coronagraph data. We were especially interested in the C2 and C3 white-light data for CMEs. C2 and C3 are two externally occulted instruments. C2 covers the range of 2 to 6 solar radii and C3, 4 to 32 solar radii (Brueckner et al., 1995). The cadence for our data was between 30 and 90 minutes.

(2) Full disk MDI magnetograms. MDI mainly obtains full-disk Dopplergrams, for the investigation of solar oscillation. However, it can obtain magnetograms with various cadence and image size (Scherrer et al., 1995). For the data used in the current study, the cadence was 90 minutes, and the pixel size was 2 arcsec.

(3) EIT FeXII 195Å full disk movies. EIT provides wide field images of the corona and transition region on the solar disk and up to 1.5 solar radii above the solar limb. It observes in 4 spectral lines: Fe IX (171Å), Fe XII (195Å), Fe XV (284Å) and He II (304Å). These lines allow imaging of solar plasmas at certain temperature diagnostics in the range 6×10^4K to 3×10^6K (Delaboudinere et al., 1995). For the two events discussed in this paper, only FeXII 195Å data were obtained continuously. The sensitivity of this line peaks between 1 and 2 MK. Cadence was 15 minutes to 1 hour, and pixel resolution was 2.5 arcsec.

2.2. BBSO Observations

(1) Full disk Hα movies. The cadence was 1 minute and the pixel resolution was 1 arcsec. The observations covered both events completely.

(2) High resolution Hα observations. They were obtained by the 65-cm reflector, with a 0.25Å Zeiss filter and an OSL (Orbiting Solar Lab) 12 bit camera. The cadence was 30 sec, pixel resolution 0.3 arcsec. This observation covered the November 5, 1998 event completely, however, it missed the start and the peak of the April 29, 1998 event.

(3) High resolution line-of-sight magnetograms, obtained by the 25-cm refractor. The pixel resolution was 0.5 arcsec, and cadence 30 seconds. The integration time of each image was 4 sec.

2.3. Yohkoh/SXT Observations

SXT is an instrument on board Yohkoh to study thermal structure of solar plasma (Tsuneta et al., 1991). For the two events analyzed in this paper, full disk Yohkoh SXT images were obtained in three filters (Al1, Al2, and AlMg, which cover a wide temperature range from 3 to 10 MK). Only partial frame images were obtained during the flares. We used standard SXT tools to de-compress the images. The cadence during those two flares was 10 minutes to 1 hour. Our analyses concentrated on the Al1 filter data, which covers the lower temperature range (about 3 MK), so they can be compared with the EIT 195Å images more easily. The pixel size of SXT images was 5 arcsec. The April 29, 1998 observation was in a nominal mode, while November 5, 1998 observation was during a CCD bakeout period, so the data had poorer quality.

2.4. Image Alignment

To compare data from several instruments, data alignment is extremely important. For this particular study, the alignment is relatively easy, as BBSO Hα, SOHO EIT/MDI/LASCO and Yohkoh SXT images were all full disk data. Alignment among these images was easily done by limb fitting. Then, the BBSO high resolution Hα images were aligned with BBSO full disk Hα images, and BBSO high resolution magnetograms were aligned with MDI full disk magnetograms. Movies were compiled and viewed for all the observing sequences. We believe that the accuracy of image alignment is better than 5 arcsec. The roll-angle correction (relative rotation of images) is better than 1 degree, they were detected by manually flicking two full disk images.

3. RESULTS

3.1. Flares

The upper panels of Figures 1 and 2 show GOES soft X-ray 1-8Å flux plots of the April 29 and November 5, 1998 flares as a function of time. Clearly, both are long duration events, lasting several hours. Lower panels show the time plots of the coronal dimming, which will be discussed later.

Figure 3 shows the development of the April 29, 1998 M6.8 flare in Hα. Filament disappearance is clearly associated with this two-ribbon flare. Two initial flare ribbons were very close (barely separable), and moved apart gradually. Only the center section of the filament disappeared during the flare. This event fits nicely with the sigmoid classification of erupting filaments and flares as proposed recently by Canfield et al. (1999).

Figure 4 shows the development of the November 5, 1998 M8.4 flare in Hα. This is also a two ribbon flare, however, there is no filament disappearance, in fact, no filament was present in this active region for the whole period that the region was on the disk. The images are from BBSO high resolution observations. The two flare ribbons were well separated initially, and moved further apart as the flare progressed.

Figures 5 and 6 show the longitudinal magnetic contours overlaid on the flare ribbons at the peak of the April 29, 1998 and November 5, 1998 events, respectively. Note that the two events are very similar in the sense that the magnetic neutral lines divide two polarities, one side includes a large sunspot, the other side just includes plage regions; both show two ribbons. For the April 29 event, both ribbons are close to the neutral line; for the November 5 event, the ribbon corresponding to the positive magnetic polarity is close to the neutral line, and the opposite ribbon is further away.

3.2. The Partial Halo CMEs

Figure 7 shows the time sequence of LASCO C2 images of April 29, 1998, with the image taken at 1527UT subtracted from each, to highlight the coronal changes. Note that even though the flare and filament eruption occurred in the South-East (SE) part of the disk, the Halo CME showed maximum intensity and extension in the North-East (NE) limb. We are convinced that the flare and the CME are related, since, in the Hα movie, filamentary materials are observed moving across the equator toward the direction of the centerline of CME, as seen in the LASCO movie. The Hα movie can be viewed in http://solar.njit.edu/ha980429.mpg. It is hard to demonstrate this motion by other methods. The motion of dark material occurred around 1635UT, towards top-left. The speed was about 100 km/s.

The CME first appears in C2 as a very bright, flattened mound in the NE at 1658 UT. There were clear extensions of this mound extending above the poles and into the west, surrounding the occulting disk. The leading edge of the CME traveled through the C2/C3 fields with a constant speed of 1,020 km/s. As this mass ejection moved outward, the sides of the mound appeared to travel faster than the center, distorting the original mound with increasing altitude. This is an example of a highly structured halo CME. At 1858UT, bright linear structured material, interpreted as being filamentary fragments, appeared in the NE and traveled slowly (110 km/s) out of the field of view, consistent with the speed of Hα filamentary material observed on the disk.

Figure 8 shows a LASCO C3 image of November 5, 1998 taken 2 hours after the flare at 2330UT, with the 1649UT image, taken 4 hours before the flare, subtracted from it. This event is likely associated with the flare, since the concentration of the CME is in the direction of the N-W limb, and the flare occurred close to that part of the limb. However, we need to be cautious that the CME source region is commonly much larger than the active region, which can be on one side of a CME (Harrison, 1995).

The CME first appears in C2 as bright mound with some internal structure in the NW at 2033 UT. Faint extensions of the mound can be detected completely surrounding the occulting disk, offset to the NW. The mass ejection traveled through the C2/C3 fields with an apparent constant speed of 1,155 km/s for the leading edge. There is also an apparent deflection of an existing streamer around the mound (to the NNW).

To estimate the onset time of the CME is difficulty, as we know that CMEs may be accelerated while moving out. So their speeds would be between 100 and 1000 km/s, when traveling between the surface source and the first appearance on C2. That would give us a 0.5 hour to 5 hours of delay between the onset and the first appearance on C2. The uncertainty is too big to give an accurate estimate of the onset time of the CME.

3.3. Coronal Dimming

Coronal dimmings associated with CMEs have recently received considerable attention. They are observed with Yohkoh SXT both as disk events (Sterling and Hudson, 1997) and limb events (Gopalswamy and Hanaoka, 1998). Thompson et al. (1998) also discovered dimming in EUV associated with CMEs from EIT/SOHO observations. Dimmings were also reported using Coronal Diagnostic Spectrometer (CDS) on SOHO (Harrison, 1997). For the two events in the current paper, we have the opportunity to study dimming simultaneously with SXT and EIT observations.

The top row of Figure 9 shows EIT 195Å images before the flare (1920UT), after the flare (1953UT) and the difference between two. Three dimming regions are marked by A, B and C in the difference image. Note that A is in the general direction that the CME moves across the disk, toward the limb. The bottom row shows pre- and post-flare, and the difference between the SXT images. It is somehow surprising that coronal dimming was not observed by the soft X-ray observations, as seen in the lower-right panel of Figure 9. The most obvious explanation is the temperature of the lost material: 195Å emission is formed at temperature around 1.5 million K and SXT observations are in the range between 2 and 4 million K. So the ejected material is probably mostly cooler than SXT can see. It also provides a hint that dimming is probably due to a loss in density, instead of a decrease in the temperature, as noted by Thompson et al. (1998). Otherwise, SXT dimming would be observed as the coronal material becomes cooler.

Figure 10 shows the similar comparison for the dimming of the November 5, 1998 event. Again, the EIT 195Å dimming is very extensive, while dimming in SXT is not visible. The primary dimming is in a large area S and SW of the AR, and marked by six area ("A" through "F").

Figures 9 and 10 also demonstrated that the direction of cusp pointing in SXT post flare images, determines the dominant direction of CMEs. For the April 29, 1998 event, it is the N-E, and for the November 5, 1998 event, it is N-W. Of course, two examples do not provide statistical meaning in this regard.

In the lower panel of Figures 1 and 2, we plot the relative dimming value in FeXII 195Å as a function of time. The value is defined as contrast integrated over all the dimming areas ("A", "B" and "C" for the April 27, 1998 event; and "A" through "F" for the November 5, 1998 event). For both events, dimming started about 2 hours before the onset of the flares, indicating that a large scale restructuring started before the flares. It is interesting to note that, for the November 5 event, the rising part of dimming covers three flares, M8.4 and two smaller events before it. Those two smaller events occurred in the same active regions but are associated with different magnetic neutral lines. An impulsive M2 flare occurred at 1830UT, is shown in the first panel of Figure 1 (lower right part of the field of view). It corresponds to the foot of the dimming area E of the in Figure 10. A very small C2 flare occurred at 1920UT, it had extended but very weak brightening over the entire active region.

As we did not have multi-wavelength EIT data to derive temperature and density of dimming plasma, it is hard to derive the mass of lost material. However, we note that our dimming area is in the same order of magnitude as the event studied by Sterling and Hudson (1997), i.e. 10^{20}cm^2. If we adopt their calculation, the dimming mass loss is about 10^{14}g. This number is one to two orders of magnitude smaller than the mass of a typical CME (Harrison, 1994, 1995). Therefore, dimming can only count for a fraction of mass in a CME.

3.4. Structure and Evolution of Magnetic Fields

Even though the scale of magnetic fields associated with flares and CMEs is not yet clear, it is believed that magnetic fields in the corona change their structure substantially after a major CME/flare event. In the flaring region, it is obvious from the Hα observations that the chromospheric fibril structure changes from a low-lying sheared configuration to higher potential-like post-flare loops in both cases. However, it is unclear if such a major change would show some signal in the photospheric magnetic fields, and what the structure of these new coronal holes would be as the result of the dimming. We used BBSO high resolution magnetograms and MDI/SOHO full disk magnetograms to search for the answer. EIT and SXT images also show substantial changes in coronal morphology. As demonstrated in Figure 9 for the April 29, 1998 event, the S-shaped sheared roped structure is obvious in the SXT pre-flare image. It forms a cusp and more of a potential configuration in the post-flare SXT image. Post flare loops are also visible in the EIT post-flare image. For the November 5, 1998 event, SXT images (Figure 10), strongly suggest that two interacting loops are visible before the flare, and show a high loop after the flare. In order to demonstrate that more clearly, we magnify SXT images and plot them in Figure 11. SXT contours are plotted over by simultaneous magnetograms, one before and one after the flare. Two loops appear to interact near point X, where strong magnetic flux cancellation was observed throughout the day. Figure 12 elaborates the detailed evolution of magnetic fields near that point. Rapid converging motions (about 1 km/s) were detected towards neutral line 2 throughout the observing period. Positive flux in neutral line 1 completely disappeared during the day. However, sudden photospheric magnetic field changes were not detected either around the active regions using high resolution BBSO data, or globally using the lower resolution MDI data. Analyses of several hours of magnetograph data show slow evolution which is not different from typical non-flare period. Even though we divided the field of view into many small windows, changes in the mean flux density in each window is always below 0.1 Gauss, below the noise level of BBSO and MDI magnetograph systems. We were especially careful in examining areas of new coronal holes as the result of dimmings, magnetic changes inside new coronal holes were not detected.

4. DISCUSSION

In many aspects, the two flares presented in this paper are very similar. However, they may represent two different energy release processes: the eruption of twisted loops (April 29, 1998 event) and the reconnection of interacting loops (November 5, 1998 event). The purpose of this paper is to show that both type of the energy release processes may be associated with CMEs. The major morphological difference is that the former event is associated with the filament eruption, and the later is not. However, it is possible that the November 5 event is associated with an erupting filament which is too hot to be seen in Hα. This is unlikely, because no filament was observed in HeII 304Å images either.

Our conclusion that the two flares are physically different is not only based on association with filament eruptions, but also based on the following additional information: the April 29, 1998 event shows a clear S-shaped sheared loop structure, which is a typical sigmoid configuration (Canfield et al., 1999) and the November 5, 1998 event shows two-loop interaction. A separate paper, submitted to Ap. J., studies this part in detail by using force-free extrapolation, which actually reveals interaction among at least 3 loops in three different stages (Yurchishin et al., 1999). For the April 29, 1998 event, a sheared magnetic configuration is clearly seen before the flare. Even though we do not know the exact helicity involved, the energy source is clearly released from the single sheared loop. For the November 5, 1998 event, two initial loops appear to be potential. Magnetic reconnection at an interacting point is responsible for release of the energy.

The EUV dimmings are quite obvious in both events. SXT dimmings are hard to detect, probably due to its dominant sensitivity to higher temperatures. So the lost material may have a relatively lower temperature – about 1.5 million degrees. Dimmings started 2 hours before flares, indicating the possibility that flares and the CMEs are products of a larger scale re-arrangement of magnetic structure.

We failed to detect any large scale or local photospheric magnetic field changes during the flares. Most importantly, no line-of-sight magnetic field changes are detected in the dimming areas. Chromospheric and coronal loops structure are observed to change locally from the more sheared to more potential form in the flare sites for both events.

We wish to thank the referee, Dr. Richard Harrison, for many valuable comments which were very helpful in improving the paper. We are grateful to the observing staff at BBSO for their support in obtaining our data. We are also grateful to the SOHO team. The work is supported by NSF under grants ATM-9628862, ATM-9714796 and ATM-9713359, NASA under grants NAG5-4919, NAG5-7350 and NAG5-7085, and ONR under grant N00014-97-1-1037.

REFERENCES

Brueckner, G.E. & 14 others, 1995, Solar Physics, 162, 357

Canfield, R.C., Hudson, H.S. & McKenzie, D.E., 1999, Geophysical Research Letters, 26, 627

Delaboudinere, J.P., & 28 others, 1995, Solar Physics, 162, 291

Domingo, V., Fleck B., & Poland, A.I., 1995, Solar Physics, 162, 1

Feynman, J. & Hundhausen, A.J., 1994, Journal for Geophysical Research & Space Physics, 99, 8451

Gopalswamy, N. & Hanaoka, Y., 1998, Ap. J. Letters, 498, L179

Harrison, R.A., 1991, Philosophical Transactions of Royal Society of London, 336, 401

Harrison, R.A., 1994, Advances in Space Research, 14, 23

Harrison, R.A., 1995, Astron. and Astrophys., 304, 585

Harrison, R.A., 1997, 'Overview of Results from IACG Campaign 3: CME Onsets', ESA SP-415, 121

Howard, R.A., Michels, D.J., & Sheeley, N.R., Jr., 1982, Ap.J. Letters, 263, L101

McAllister, A.H., Dryer, M., McIntosh, P., Singer, H. & Weiss, L. 1996, Journal of Geophysical Research, 101, 13

Plunkett, S.P, Thompson, B.J., Howard, R.A., Michels, D.J., St. Cyr, O.C., Tappin, S.J., Schwenn, R. & Lamy, P.L., 1998, Geophysical Research Letters, 25, 2477

Scherrer, P.H. & 12 others, 1995, Solar Physics, 162, 129

Sterling, A. & Hudson, H.S., 1997, Ap. J. Letters, 491, L55

Thompson, B.J., Plunkett, S.P., Gurman, J.B., Newmark, J.S., St. Cyr, O.C., & Michels, D.J., 1998, Geophysical Research Letters, 25, 2465

Tsuneta et al., 1991, Solar Physics, 136, 37

Verma, V.K., 1990, IAU Symposia, 142, 450

Yang, G. & Wang, H., 1999, BAAS, 31, 854

Yurchishin, V, Wang, H., Qiu, J., Goode, P.R. & Abramenko, V.I., 1999, Ap.J., submitted

Zarro, D.M., Sterling, A.C., Thompson, B.J., Hudson, H.S. & Nitta, N., 1999, Ap. J. Letters, 520, L139

This manuscript was prepared with the AAS LATEX macros v4.0.

Table 1. PARAMETERS OF TWO FLARES

FLARE	04/29/98	11/05/98
Start Time	1606UT	1900UT
Peak Time	1637UT	1955UT
X-ray Class	M6.8	M8.4
Disk Location	S18 E20	N22 W18
Two-Ribbon	Yes	Yes
Filament Eruption	Yes	No
CME	Partial Halo	Partial Halo

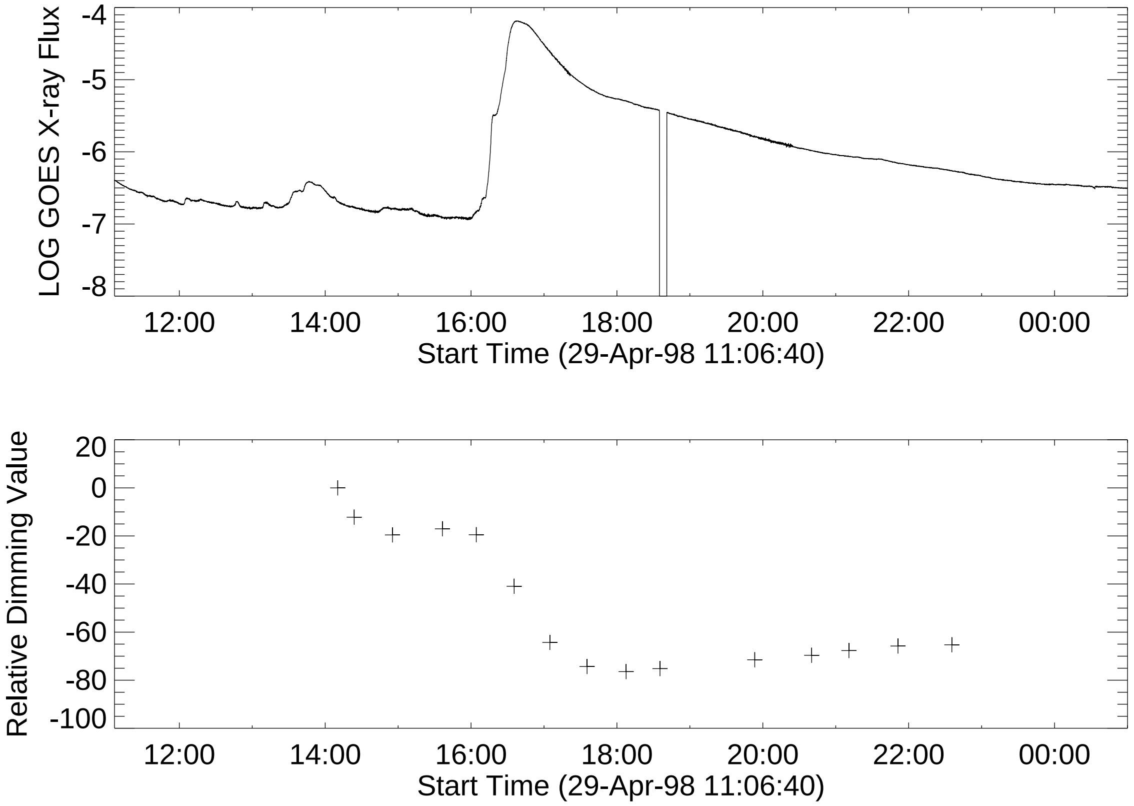

Fig. 1.— Top panel: GOES X-ray time profile of April 29, 1998 flare. Bottom panel: EUV dimming of the flare. The value is the contrast integrated over the entire dimming areas, in the unit of 10^{17}cm^2.

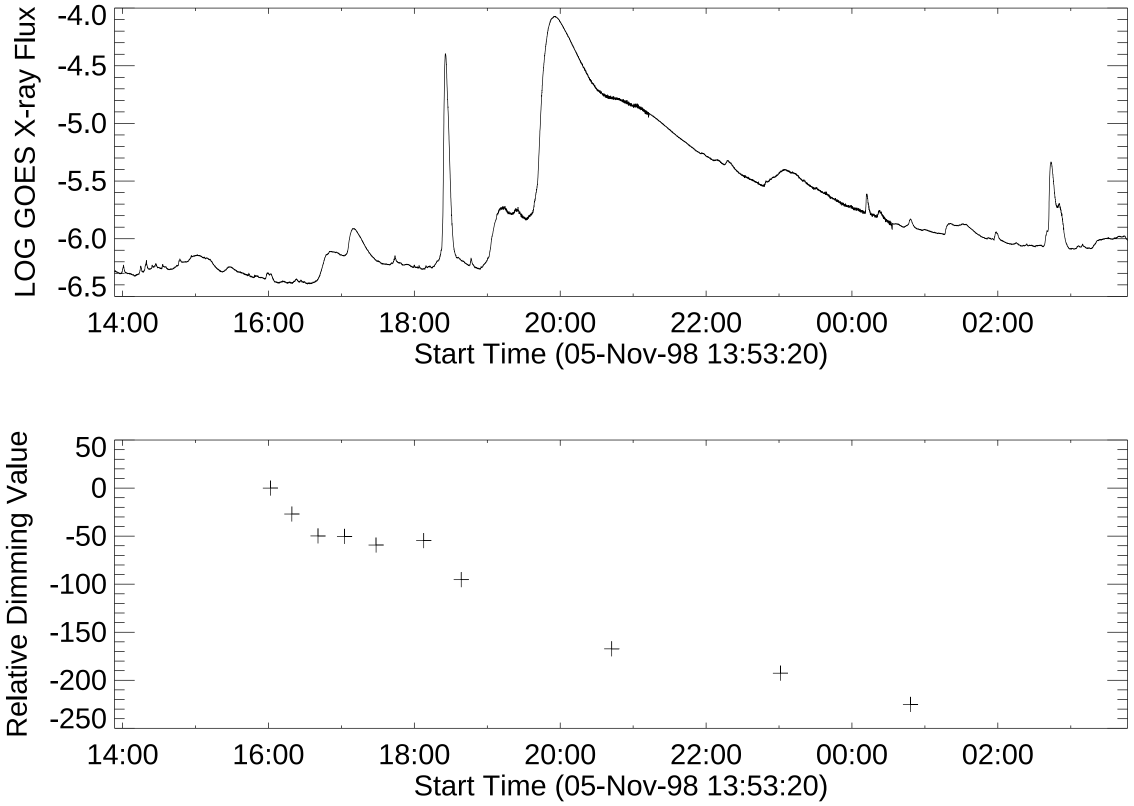

Fig. 2.— Top panel: GOES X-ray time profile of November 5, 1998 flare. Bottom panel: EUV dimming of the flare. The value is the contrast integrated over the entire dimming areas, in the unit of $10^{17}\mathrm{cm}^2$.

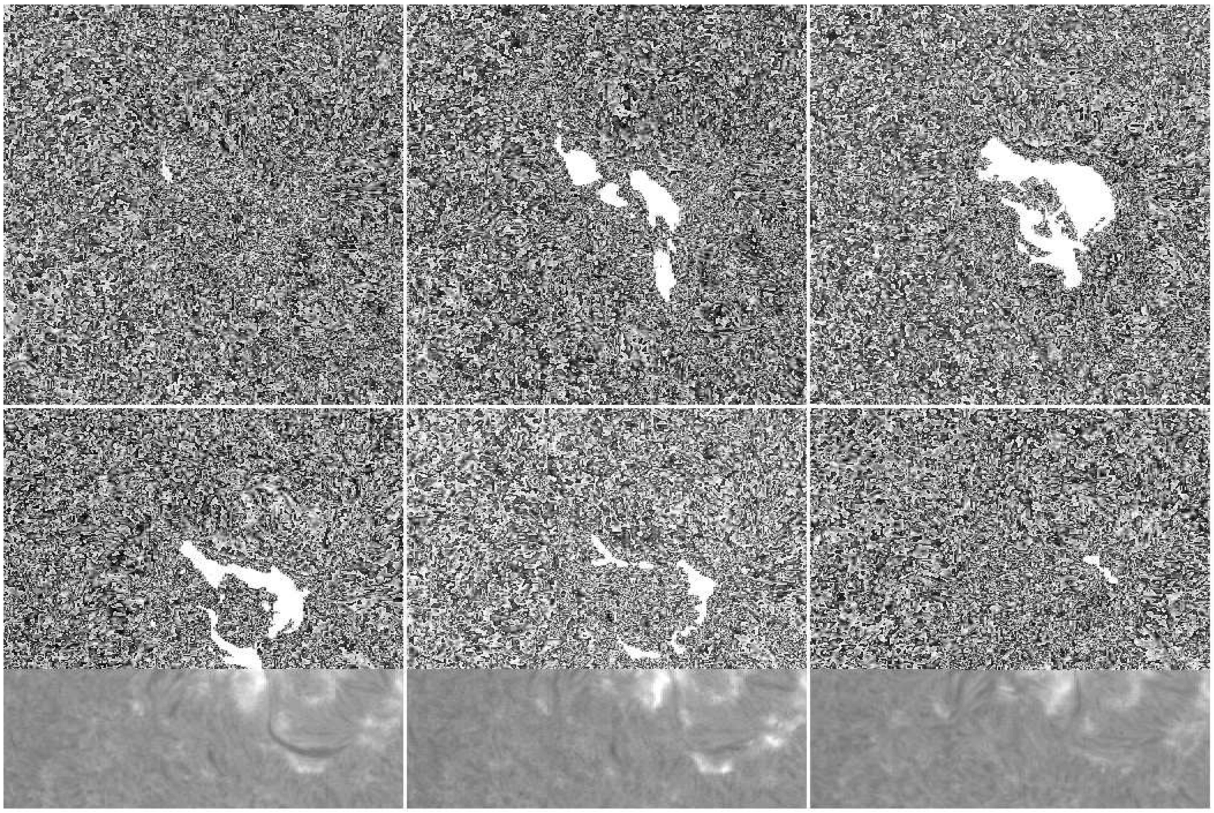

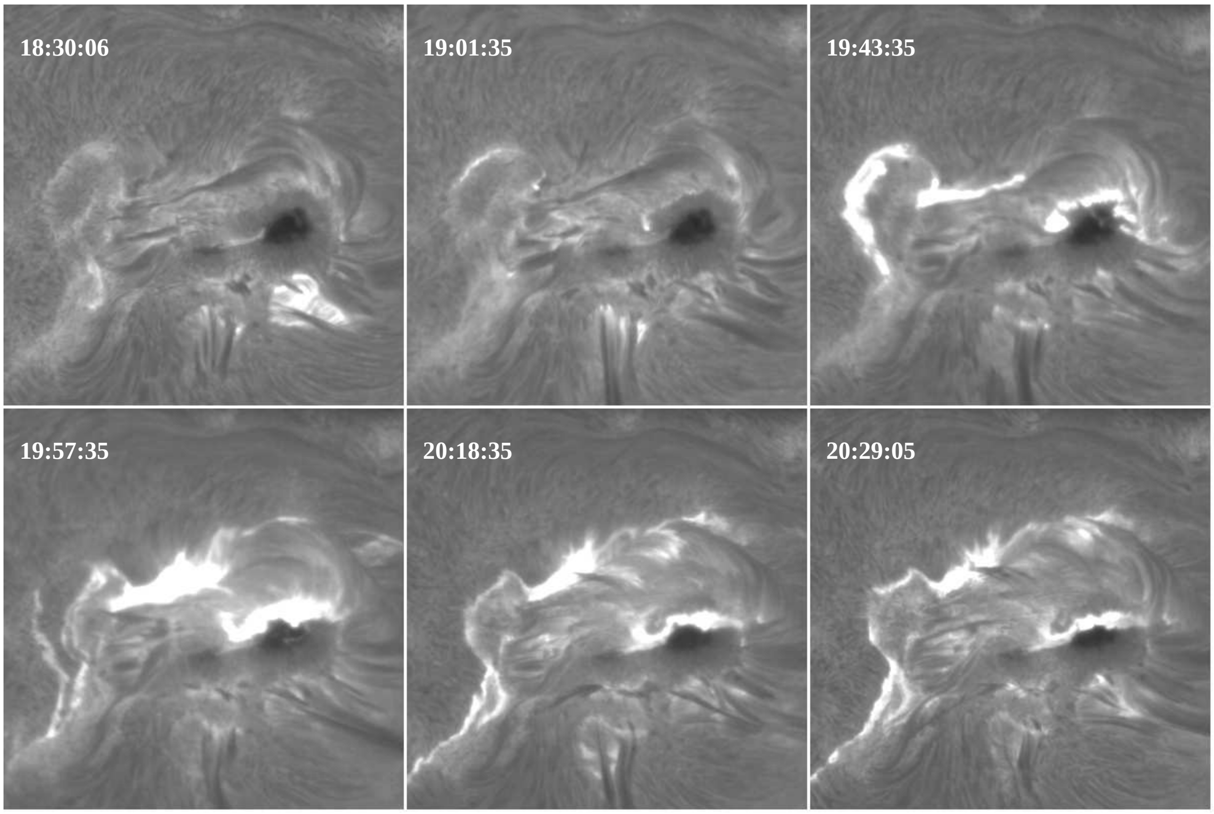

Fig. 4.— Time sequence of Hα observations of November 5, 1998. The images are from 65-cm telescope, the field of view is 200 by 200 arcsec.

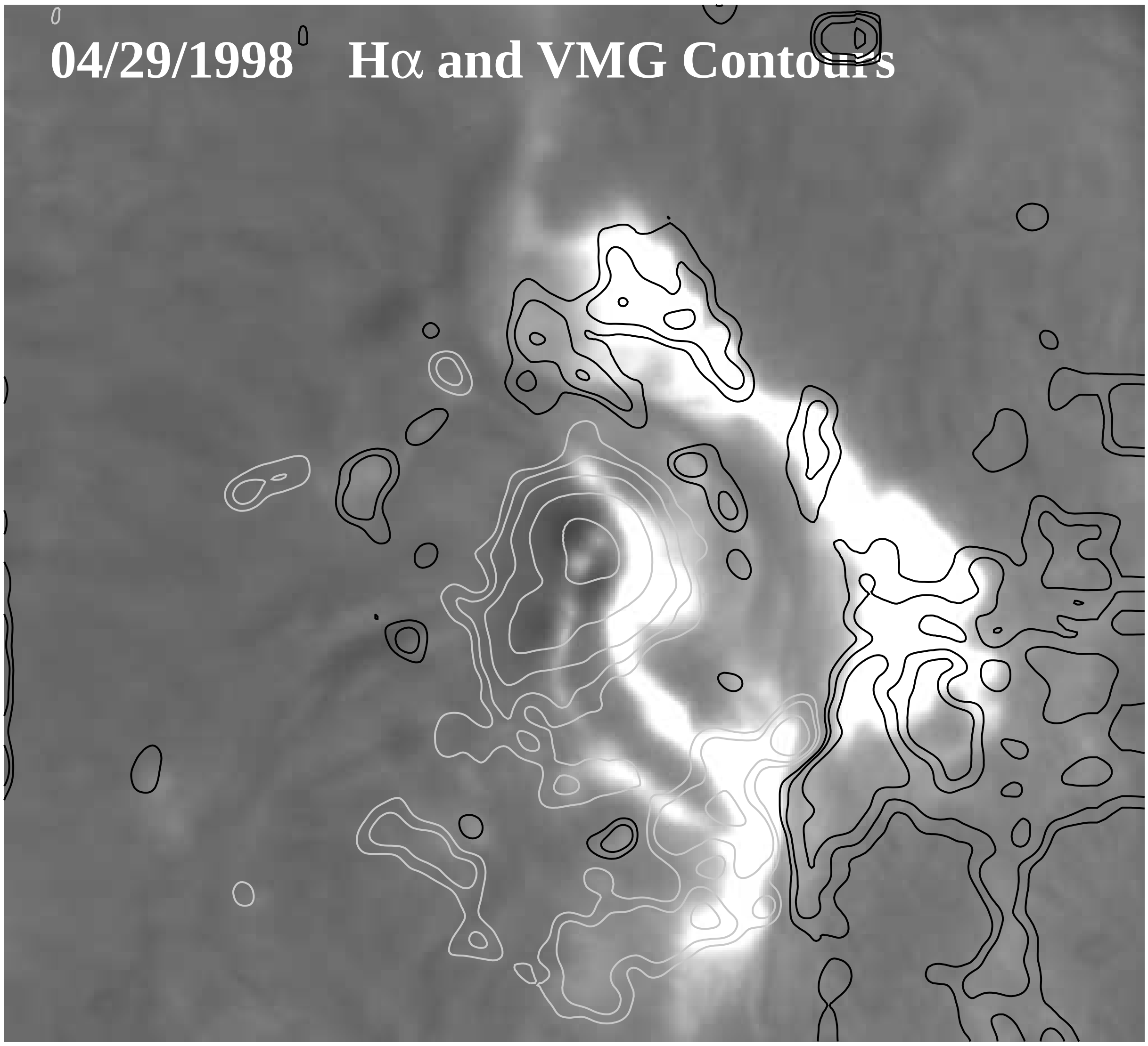

Fig. 5.— Hα image at the peak of the flare of April 29, 1998, superposed on smoothed magnetogram. White contours, positive fields, and black contours, negative fields. Contour levels are 100, 200, 400 and 800 Gauss.

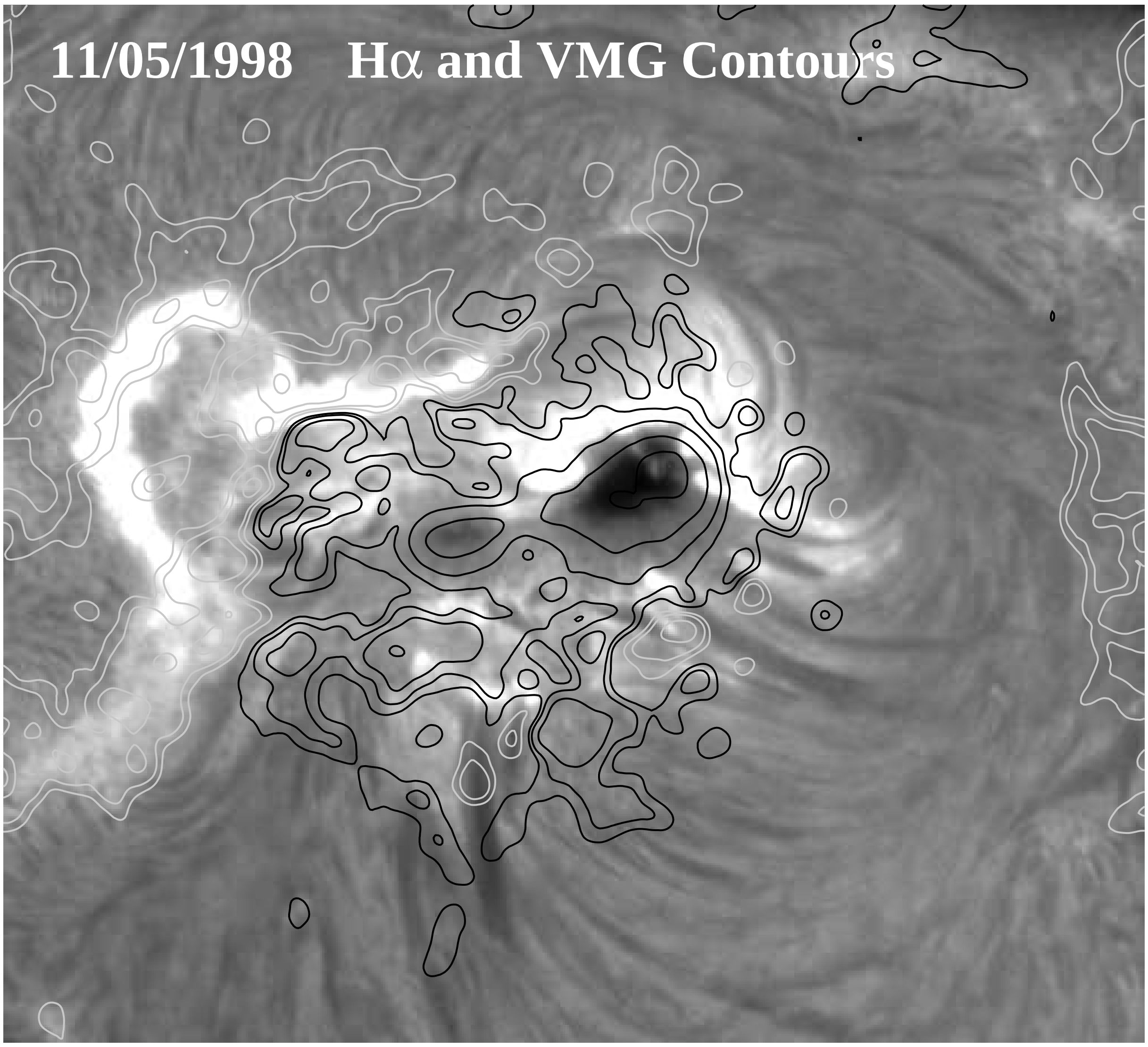

Fig. 6.— Hα image at the peak of the flare of November 5, 1998, superposed on smoothed magnetogram. White contours, positive fields; and black contours, negative fields. Contour levels are 100, 200, 400 and 800 Gauss.

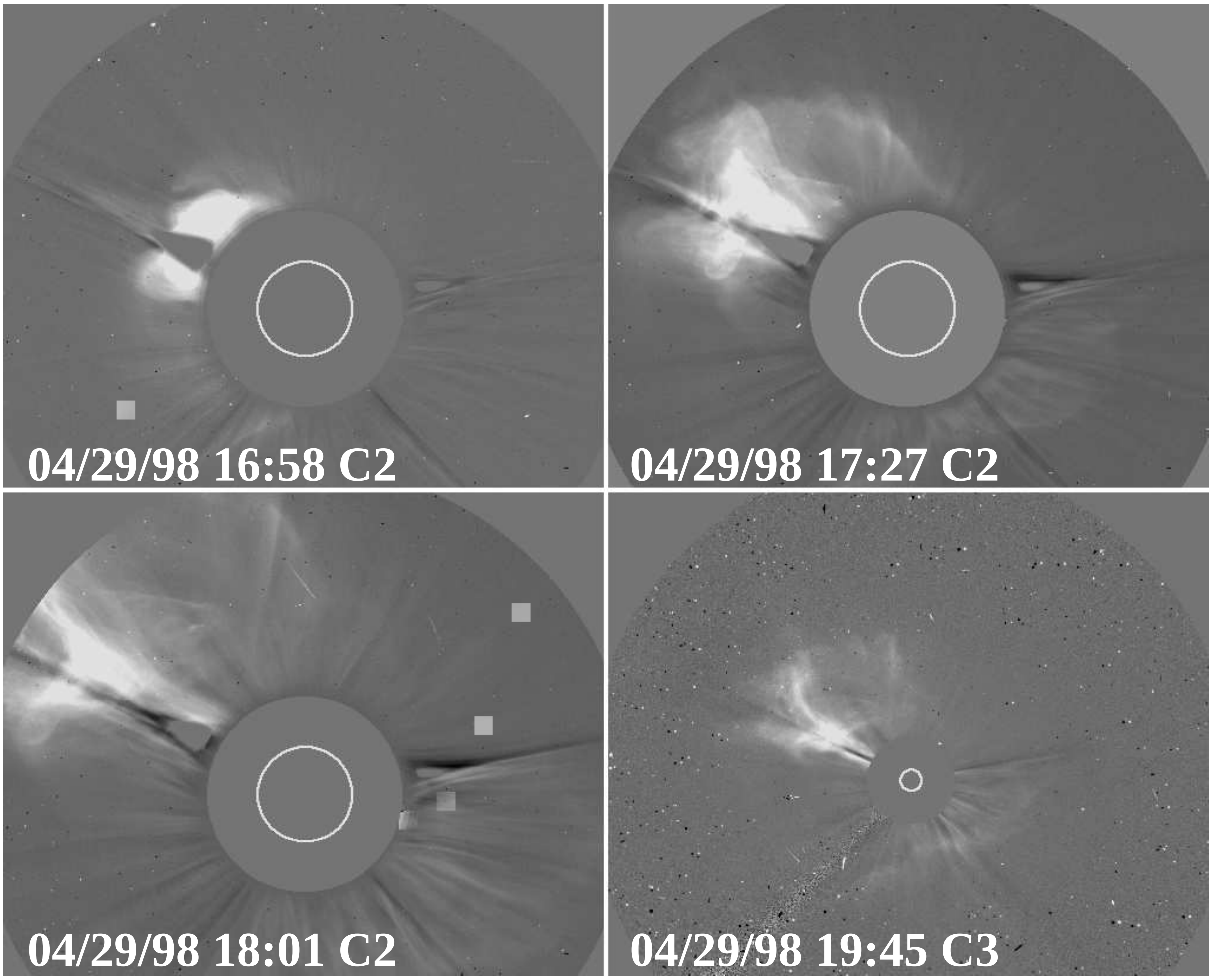

Fig. 7.— A sequence of LASCO C2 images subtracted by a reference images at 1542UT. Top is North and Left is East, the same for all the figures in this paper.

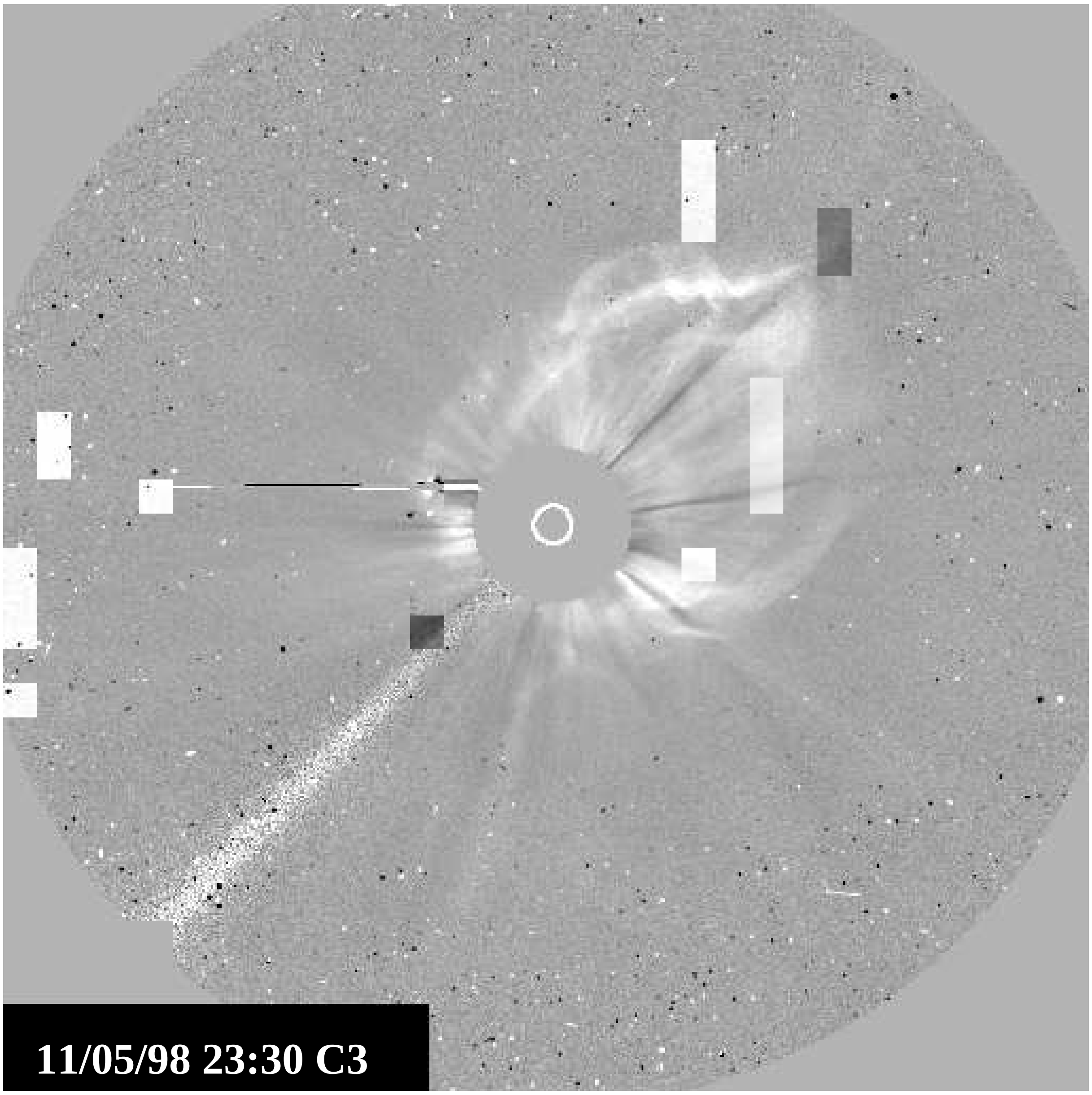

Fig. 8.— A LASCO C3 image at 2330 UT subtracted by a reference image at 1649UT.

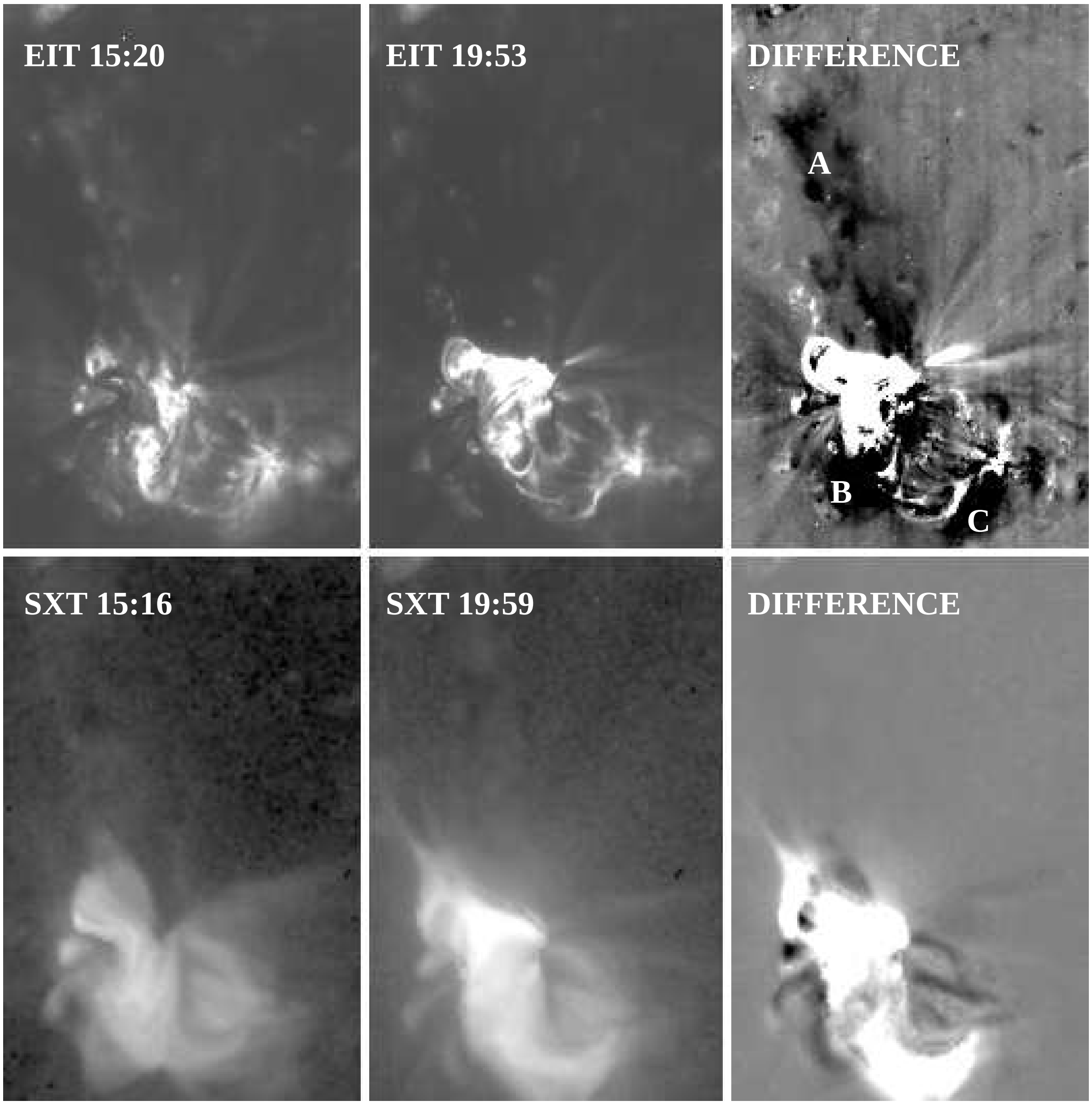

Fig. 9.— Top row: pre- and post-flare EIT 195Å image and the difference, showing the EUV dimming associated with the April 29, 1998 flare/CME. Three dimming regions are marked by A, B and C. Bottom row: pre- and post-flare SXT images and the difference, showing the lack of corresponding dimming. The field of view is 350 by 530 arcsec.

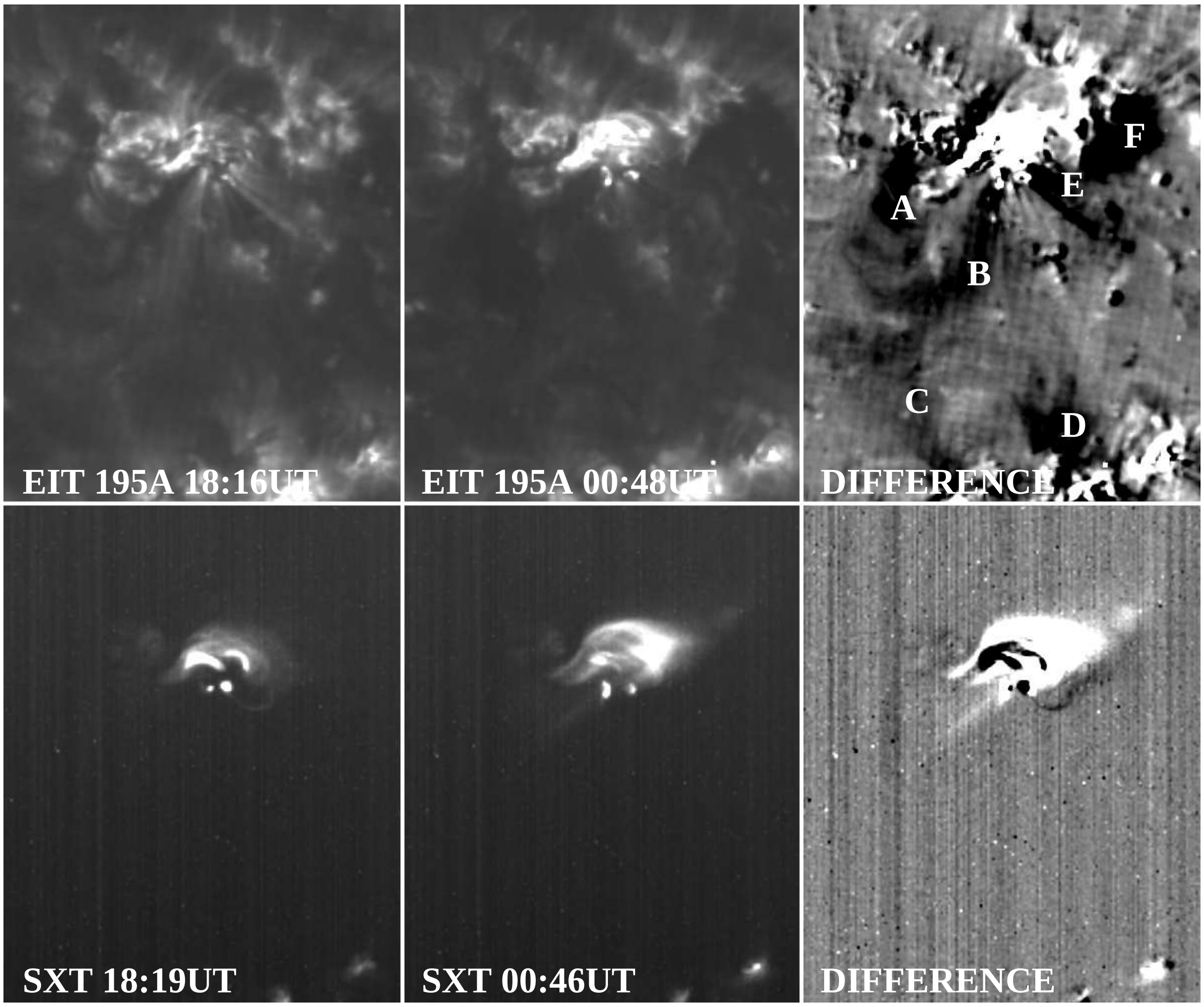

Fig. 10.— Top row: pre- and post-flare EIT 195Å images and the difference, showing the EUV dimming associated with the November 5, 1998 flare/CME. Bottom row: pre- and post-flare SXT images and the difference, showing the lack of corresponding dimming. The field of view is 580 by 1000 arcsec.

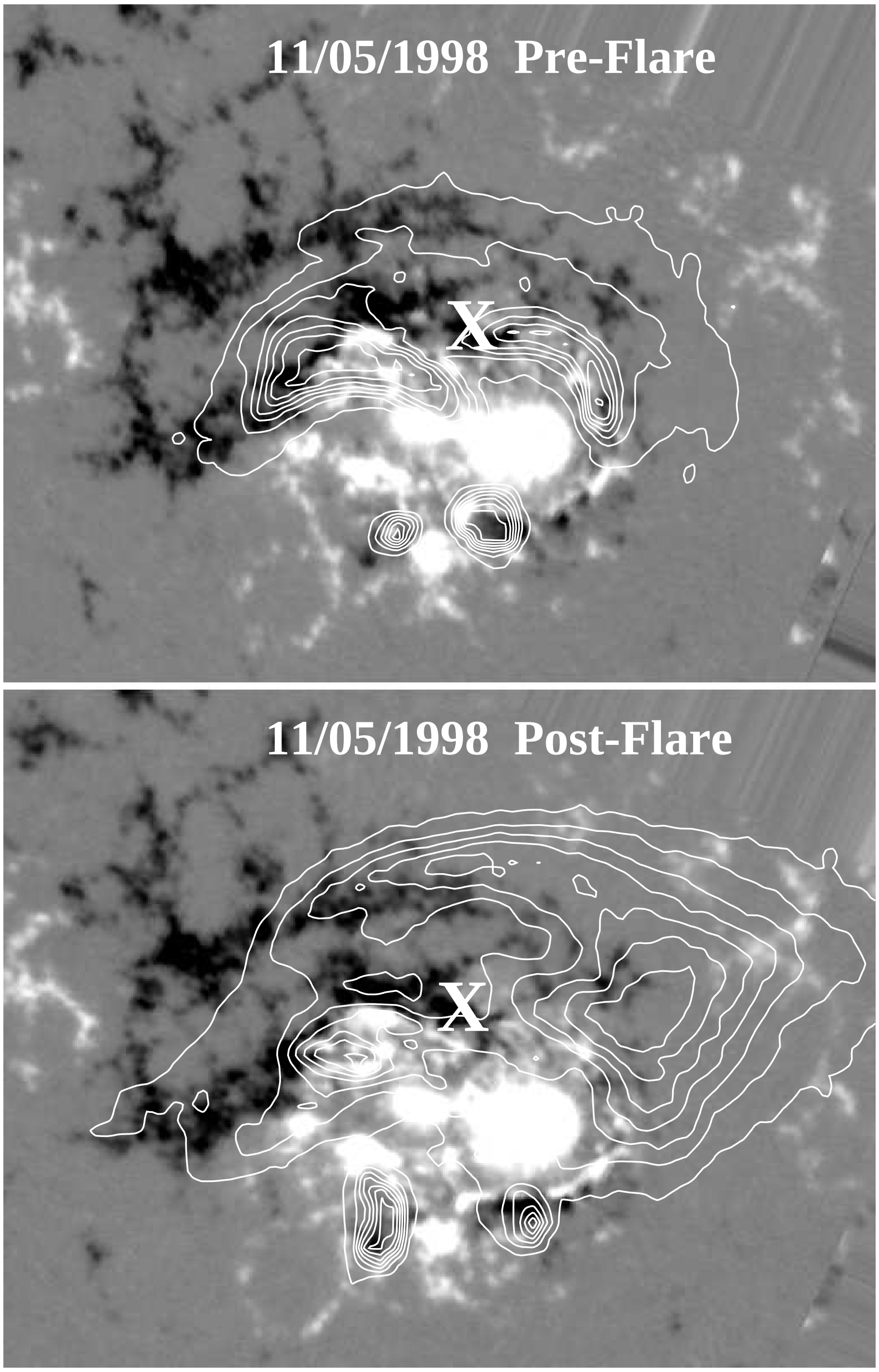

Fig. 11.— SXT contours superposed on corresponding magnetograms on November 5, 1998. The upper panel is the preflare image at 1818UT and lower panel is the post-flare image at 2258UT.

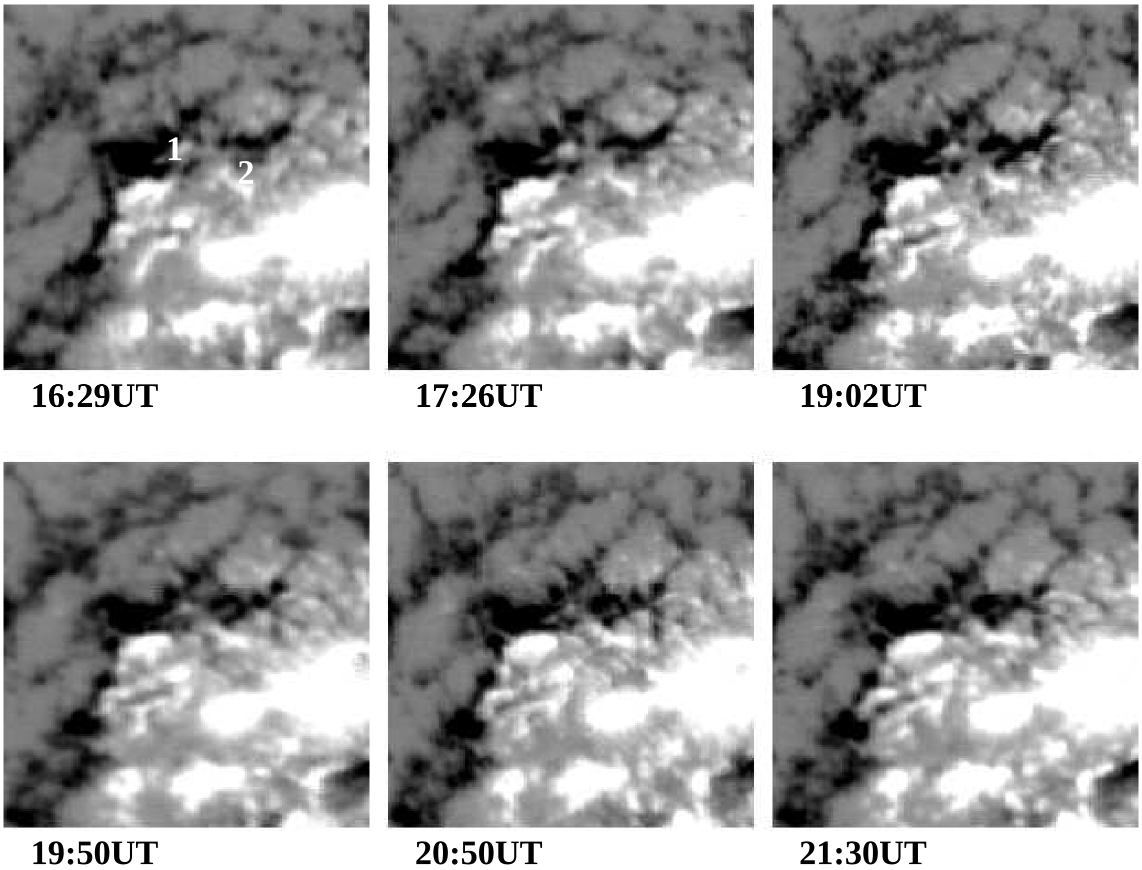

Fig. 12.— Evolution of magnetic fields, showing converging motion and flux cancellation near the contacting point of two loops which is demonstrated in Figure 11. 1 and 2 are two converging neutral lines. The field of view is 100 by 100 arcsec.